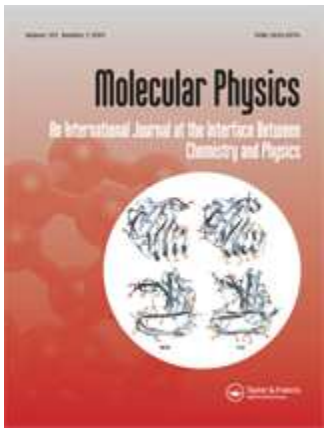

Rapid passage induced population transfer and coherences in the 8 micron spectrum of nitrous oxide

Journal:	*Molecular Physics*
Manuscript ID:	TMPH-2006-0089.R1
Manuscript Type:	Full Paper
Date Submitted by the Author:	17-Dec-2006
Complete List of Authors:	Duxbury, Geoffrey; University of Strathclyde, Department of Physics Langford, Nigel; University of Strathclyde, Physics McCulloch, M; Strathclyde University, Physics Wright, S; University of Strathclyde, Physics
Keywords:	

Rapid passage induced population transfer and coherences in the 8 micron spectrum of nitrous oxide

G. Duxbury, N. Langford, M. T. McCulloch and S. Wright,

Department of Physics, John Anderson Building, University of Strathclyde, 107 Rottenrow East Glasgow, Scotland G4 0NG
G.Duxbury@strath.ac.uk

Abstract: Rapid passage signals showing the effects of molecular alignment have been observed when low pressure samples of nitrous oxide are interrogated by radiation from a pulsed 7.84 μm quantum cascade laser. These effects occur when the sweep rate of the laser through a Doppler broadened absorption line is much faster than the collisional relaxation time, and when the power density of the linearly polarised laser radiation is sufficient to cause optical pumping. Using a laser pulse of duration 1.3 microseconds, the frequency sweeps approximately 90 GHz. The variation of the laser tuning rate during the laser pulse, from about100 MHz/ns at the beginning to about 20 MHz/ns at the end, allows the relationship between sweep rate and collisional damping to be investigated. We show, by comparing the experimental signals with those calculated by coupled Maxwell-Bloch equations, how the rapid passage effects in nitrous oxide are influenced by the number density, transition cross-section and reorientation lifetime.

Introduction

We have recently demonstrated [1] that the frequency swept output from pulsed quantum cascade (QC) lasers is a very efficient way of producing coherent excitation of vibration rotation transitions in the non-polar molecule ethylene. These signals were observed in fast passage experiments in which the rate of frequency sweep, or chirp, through a Doppler broadened absorption line is faster that the collisional relaxation. The experiment used a 10.24 μm frequency down-chirp quantum-cascade laser based spectrometer, in which the laser radiation chirped rapidly from high to low frequency, and passed through a long path length cell containing ethylene at very low pressures. The strength of the observed rapid-passage signals was shown to depend greatly upon the transition dipole moment of the vibration-rotation transition, and the pressure dependence of the signals showed evidence for power saturation. In

these experiments the chirp rate of the laser was very rapid, ca. 300 MHz/ns, and the duration of the laser pulse a maximum of 300 ns.

Changing the gas to be studied from the complex spectrum of ethylene to the more open structure of the 7.84 μm spectrum of nitrous oxide [2,3] has allowed us to examine the rapid passage effects in much more detail using the intra-pulse method. In this method the tuning range and rate depend upon the frequency down-chirp of the QC laser. The chirp is caused both by the heating of the laser by up to 20^0 C during the current pulse, and also the heat transport from the active region to the Peltier-cooled heat sink. During the longer current pulses of up to 2 μs used with the more efficient 7.84 μm laser, the down-chirp varied from approximately 100 MH/ns at the beginning of the scan to ca. 20 MHz/ns at the end.

Within a typical tuning range of ca. 3 cm^{-1} obtained using a 1.3 μs current pulse, three successive strong P branch absorption lines, belonging ν_3 (3_0^1)vibration-rotation band of nitrous oxide,[3] may be observed, as shown in Figure 1. Using a laser temperature of 2 ^{0}C, the lines observed are P10, P11 and P12, see Fig 1(a) [2-5]. Since these lines lie in different regions of laser chirp rate, the time taken to sweep through a Doppler broadened half width of the highest frequency line, p10, is about 1 ns, whereas the sweep time through the lowest frequency line, P12, is about 4 ns. The typical rapid passage shape of the P12 transition is shown in Fig. 1(b) on an expanded scale.

Deleted:

Deleted:

Owing to the long pathlength within the absorption cell, up to 110 m, a range of hot band lines and weak transitions due to isotopomers may also be seen. The most prominent of these are three *l*-doublets which are members of the 01^11-01^10 ($2_1^1\ 3_0^1$) hot band. These may be seen as weak

signals approximately equidistant in frequency between the main P branch lines in Fig. 1. The reduced chirp rate of the 7.84 μm QC laser from that of the 10.24 μm laser used in the earlier experiments has allowed most of the *l*-type doubling splittings to be resolved.

In addition to these lines a variety of other transitions have been identified when the nitrous oxide pressure is increased. These are due both to weak hot bands derived from higher vibrationally excited states and also to those associated with vibration-rotation lines of the ν_3 bands of ^{15}N and ^{18}O, and ^{17}O isotopomers of nitrous oxide. The lines identified in this study are listed in Table 1.

Our ability to study such a wide variety of transitions within the tuning range of the laser has allowed us to investigate the role of number density and collision frequency in determining the type of rapid passage signal seen. Since we use very long path lengths of up to 110 m in the multiple pass absorption cells, the gas pressure of nitrous oxide used is very low, typically in the range from 0.1 to 30 mTorr (13 μPa to 4.0 mPa), whereas the time taken to sweep through a Doppler broadened line half width of 80 MHz varies from approximately 1 to 4 ns. This is much shorter than the time between collisions in the cell when pure nitrous oxide is used. The time between collisions ranges from 0.5 msec at a pressure 1 mTorr to 1.7 μs at 30 mTorr. As a result of this long period between collisions, and also the fast laser frequency sweep, the rapid passage signals observed within the cell result from weakly damped driving of the molecules between the lower and upper levels of the appropriate pair of energy levels. However the observed rapid passage signals [2], shown in Figure 1, do not show the oscillatory structure expected from a weakly damped motion of the type seen in NMR spectra [6]. We will show that the lack of

Deleted: faster than the gas collision frequency within the cell.

oscillatory structure results from two processes, the inhomogeneous Doppler broadening of the absorption line which produces phased array excitation [1,2], and the optical pumping of the different M_J components of each velocity component of the Doppler broadened line [7.8], which occurs owing to the linear polarisation of the QC laser. Such optical pumping [9] has been demonstrated to produce strong alignment effects in infrared laser pumped submillimetre gas lasers at gas pressures and radiation power densities similar to those used in the current experiments. In order to achieve such strong optical pumping and optical alignment the effect of any M_J changing collisions must be quite small.

2 THEORY: MODELLING THE RAPID PASSAGE SIGNALS

As we discussed in our study of the rapid passage signals in ethylene [1], the low pressure rapid passage signals recorded using the intra-pulse QC laser spectrometer [2,5,10] are similar to those observed in the electron spin resonance (ESR) spectra of inhomogeneously broadened samples, where the inhomogenous broadening is due to magnetic field inhomogeneity [11]. In our gas phase experiments the absorptions lines are inhomogeneously broadened due to the Doppler effect[1,2]. During the frequency sweep of the laser, each homogeneously broadened velocity component of the Doppler broadened line is interrogated sequentially, so that the velocity packets are excited as a phased array [1,2].

Deleted:

Deleted:

The principles of our analysis, using the Maxwell-Bloch equations [12], have been described previously [1,2]. Each transition is treated as a simple two level system with a resonance frequency ω_a. The rate at which population may decay from the upper to the lower level is γ_1. Making the electric dipole approximation, the coupling of the field to the transition results in the

formation of a dipole that dephases from the driving field at a characteristic rate γ_2. The evolution of this dipole can be described by the Bloch vector which has components u(t), v(t) and w(t). The components u(t) and v(t) relate to the complex refractive index, χ, whilst the w(t) term quantifies the population difference between the upper and lower levels of the transition. In the Maxwell-Bloch equations [12] the electric field may be represented by a plane polarised travelling wave along the z axis,

$$E(t) = 2E\cos(\omega t - kz) \tag{1}$$

where k is the wavenumber, and induces a macroscopic dipole moment, or polarisation, in the two level system. The polarisation may be written as

$$P(t) = \left(P_r(t) + iP_i(t)\right)e^{i(\omega t - kz)} + cc, \tag{2}$$

where cc is the complex conjugate. If the number density of the two level system is *N*, for a linear frequency chirp α, and the detuning Δ, the evolution of the polarisation *P* and the population inversion *w* for a velocity component v_z is given by

$$\begin{aligned}
\frac{dP(t,v_z)}{dt} &= -i\Delta(t)P(t,v_z) - \gamma_2 P(t,v_z) - i\frac{N\mu_{12}^2}{\hbar}E(t)w(t,v_z),\\
\frac{dw(t,v_z)}{dt} &= -\frac{2i}{N\hbar}\left(E(t)P(t,v_z)^* - E(t)^*P(t,v_z)\right) - \gamma_1\left(w(t,v_z) - w_{eq}\right),\\
\frac{dE(t)}{dz} &= \frac{ik}{2\varepsilon_0}\int P(t,v_z)dv_z,\\
\Delta(t) &= \omega_a - (\omega_i + \alpha t)
\end{aligned} \tag{3}$$

where ω_i is the starting frequency, γ_1 is the longitudinal (population) decay rate, γ_2 is the transverse (polarisation) decay rate and ε_0 is the relative permittivity of free space. The on-resonance Rabi frequency, in angular frequency, Ω_{12}, which represents the cycling between the upper and lower states, is expressed in terms of the transition dipole moment, μ_{12}, and the field as,

$$\Omega_{12} = \kappa E$$
$$\kappa = \frac{\mu_{12}}{\mathrm{h}} \qquad (4)$$

where the field amplitude $E = \sqrt{\frac{2I}{\pi\varepsilon_0 c r^2}}$ with I the peak output power, r the e^{-1} width, mode waist, of the electric field distribution and c the speed of light of free space.

In our study of ethylene [1] we used a single transition dipole moment for each vibration-rotation transition. However as the QC laser radiation is linearly polarised, in order to account for the effects of optical pumping [7,8,9] allowance should be made for the projection of the molecule-fixed transition dipole on to the space-fixed direction of the laser field [13]. The resultant direction cosines depend upon the quantum number M_J, where $M_J(\max)$ is the minimum of J' and J" [7,8]. In the absence of magnetic fields there are $M_J(\max)$ degenerate transitions, and one non-degenerate transition having $M_j = 0$, for each vibration-rotation transition. This leads to $M_J + 1$ effective transition dipole components for each vibration rotation transition, assuming that the selection rules are $\Delta M_J = 0$ [7,8,13,14]. For the fundamental ν_3 bands, and a particular value of M_J, the effective transition dipole is given by [14]:

$$\left\langle \mu_{\nu_3 \leftarrow 0} \right\rangle_{M_J} = \left\langle \mu_{\nu_3 \leftarrow 0} \right\rangle \frac{\left(J^2 - M_J^2\right)^{1/2}}{\left[(2J-1)(2J+1)\right]^{1/2}} \qquad (5)$$

The alignment of nitrous oxide is sketched in Figure 2. Since the transition dipole is perpendicular to the direction of $\vec{J}$, the maximum coupling occurs for low values of M_J as then the transition moment is almost parallel the polarisation axis, Z, of the laser radiation.

Deleted: ,

Deleted: a

We have tried two approaches to this calculation, the first involves using all the $M_J + 1$ effective transition dipole components as described above, and a second "bundled" M approach. In the latter method each transition is assumed to comprise a limited number of two levels systems, each of which interacts independently with the laser field. The number limit is the bundle number. Each bundle member then has an effective transition moment derived from the vibrational transition moment multiplied an average direction cosine. This is derived by taking a weighted average of the squares of the appropriate direction cosines related to the spread of M_J values in each component of the bundle. The sum of these bundled direction cosines is required to be equal to the sum of the squares of the complete set of direction cosines for the same vibration-rotation transition.

In solving these equations numerically we have assumed that, as the laser chirp rate varies slowly across a single absorption line or *l*-doublet, we may use a linear chirp rate. We have also assumed a constant peak power and a constant mode waist in the absorption cell. We have set the initial polarisation $P(t=-\infty)=0$, and the initial population difference $w(t=-\infty)=-1$. The values of the pressure broadening parameters of nitrous oxide for self [4] and nitrogen broadening [4] are given in Table 1, as is the ν_3 vibrational transition dipole moment [4] . We further assumed, following the microwave studies of McGurk et al. [15], that the pressure dependence of the two dephasing rates, γ_1 and γ_2, was identical. At low pressures of nitrous oxide and nitrogen in the absorption cell the homogeneous pressure broadening is much smaller than the Doppler broadening. This inhomogeneous process is taken into account by treating each velocity component as an individual emitter and the total response over the inhomogeneous line is determined by summing over all the emitters. Thus the total response, the sum of all the

Formatted: Font: Italic

Deleted:

individual emitters, is equivalent to that of a phased array. By comparing the signals calculated neglecting the inhomogeneous broadening with those allowing for the phased array behaviour, we have shown that the dephasing associated with all identical emitters causes a strong damping of the oscillatory structure [2]. All the oscillatory structure calculated using the present model includes the damping due to the inhomogeneous line broadening.

In our calculations of the variation of the polarization of a two level system, or a set of two level systems as the radiation propagates through the absorption call we have used a step length of 1 m, and a total path length of up to 80 m. At each step in the propagation of the laser radiation we have evaluated the cumulative polarisation by incoherent addition of the contributions of the M_J components. Based upon the degree of polarisation achieved in optically pumped gas lasers, as described previously, we have assumed that we may neglect the effects of M_J changing collisions. In the case of transitions between the *l*-doublets, we have added coherently, or incoherently, the equivalent M_J components of the pair of transitions, before evaluating the cumulative polarisation as above.

Deleted: We

3 EXPERIMENTAL

The spectrometer used in this work has been described in detail previously [1,5,10]. The distributed feedback QC laser, designed to operate at 7.84 μm, was supplied by Alpes Lasers. It was housed in an evacuated enclosure and excited by a rectangular current pulse with duration extending from 0.5 to 2 μs. The pulse repetition frequency ranged from 5 to 20 kHz, and the laser drive current from 2.5 to 3.5 A.

The substrate temperature of the QC laser was maintained at a constant value, close to 0 ^{0}C via a Peltier thermoelectric cooler. The spectral output from the QC laser had a temperature-tuning characteristic of -0.093 cm^{-1} K^{-1}. The QC radiation was collected by an off-axis paraboloid and coupled into the absorption cell that contains and astigmatic Herriot mirror arrangement [16]. The path lengths used in the present studies were designed to give path lengths of 40 and 110 m.

After traversing the cell the light from the QC laser was then coupled on to a small area photovoltaic mercury cadmium telluride (MCT) detector. This has an element with a diameter of 0.5 mm and an effective bandwidth of greater than 400 MHz. The electrical signal produced by the detector was amplified by 2 GHz bandwidth AC coupled amplifier, and following the amplifier sent to a computer controlled digitiser with a digitisation step size of 0.5 ns. The transient digitiser used in this work enabled the sequential collection and averaging of up to 64,000 pulses.

The operation of the spectrometer relies on the local heating induced in the QC laser by the current pulse generating an optical pulse with a frequency down-chirped spectrum. To quantify the frequency swept output from the laser, a solid Ge etalon, with a free spectral range of 0.05 cm^{-1}, was inserted between the QC laser enclosure and the cell. This etalon was mounted on a translation stage such that it could be moved into and out of the QC laser beam to allow for periodic calibration of the QC laser output during the course of a sampling cycle.

In addition to the local heating induced by the applied current pulse, it was found that the start frequency of the swept emission could be varied by changing the substrate temperature. The frequency down-chirp associated with the laser was found to vary in a non-uniform fashion across the temporal profile of the pulse and depended on the amplitude of the current pulse and substrate temperature [2,5,10]. It is known that the spectral resolution of the instrument scales as the square root of the frequency chirp [10], so that if the chirp rate slows by a factor of four during the current pulse the resolution improves by a factor of two as may be seen in Fig. 3.

4 RESULTS

Formatted: Line spacing: Double

In the typical wide-scan spectrum of a low pressure sample of nitrous oxide, shown in Figure 1, the line shape of the normalised transmission spectrum appears to have absorption followed by emission, which is characteristic of rapid passage behaviour. This may be clearly seen in figure 1(b) where some oscillatory structure following the emission peak may be seen on the expanded plot of the P 12 line. A survey spectrum, using a higher pressure of nitrous oxide, is shown in figure 3. From the large number of vibration-rotation transitions identified, as shown in Fig 3(b), it may be seen that a variety of different types of non-degenerate and degenerate transitions may be probed by choosing the appropriate cell pressure.

In order to explore in more detail the relationship between the structure of the rapid passage and the sweep rate, the P9 to P12 vibration rotations transitions of the ν_3 band of nitrous oxide have been studied in some detail. Since these are four successive members of the P branch with integrated intensities which increase slowly as J" is increased, we have used a representative

member of this series, P10, in our calculations. In Figure 4 the shape of the experimental rapid passage signal of the ν_3 P10 transition is shown in two pressure regimes, using a down-chirp rate of 23 MHz/ns. The transform limited resolution [10] obtained is 102 MHz, full width at half height. In Figure 4(a) where the pressure is very low, it may be seen that the signal resembles that of Figure 1 (b), but with most of the oscillatory structure suppressed. The resultant signal is that of rapid passage in an inhomogeneously broadened line. As the maximum pressure is 0.5 m Torr (0.067 Pa), no collisions occur within the duration of the rapid passage scan through an absorption line. In Figure 4(b), where the nitrous oxide pressure is increased to almost 10 mTorr (1.33 Pa), a much more complex type of rapid passage behaviour is observed. The absorptive part allows transmission of radiation even at a pressure range when in a continuous absorption experiment no light would be transmitted, and becomes very asymmetric as the gas pressure is increased. The part which appears as emission may have an amplitude which is two to three times larger than the power emitted by the QC laser at that frequency.

The calculated rapid passage behaviour of the response of the P(10) transition nitrous oxide using a path length of 80 m, including the phased array effect of the Doppler broadened line, and the inclusion of the 10 M_J components, is shown in Figure 5. The QC laser sweep rate, from high to low frequency, was taken to be 20 MHz/ns, the laser power 30 mW, and the beam waist 0.1 mm, all the other parameters are given in Table 2. In Figure 5(a) the calculated rapid passage signals are displayed for low pressure of nitrous oxide. It may be seen that the experimental spectra are very similar to those observed. It has been found that in this pressure regime the line shape is almost identical whether the bundled-M_J or full M_J calculation is used. If a shorter path

Deleted: 20

length of 20m is used in the calculation, with an increased gas pressure to give the same total absorbance, more damping is seen as the collision frequency has increased.

The calculated behaviour at higher gas pressures, shown in Figure 5(b), is similar to that displayed in Figure 4(b). At pressures sufficient to prevent transmission in experiments using a slowly scanned laser the absorptive part of the transmission spectrum becomes very asymmetric, with a switch from absorption to emission whose delay increases as the gas pressure is increased. The height of the calculated emission "spike" also increases with increased nitrous oxide pressure. The main difference between the calculated and observed behaviour is that the calculations predict more oscillatory structure following the spike than is observed experimentally in Figure 4(b).

In order to understand the reasons for this behaviour we have analysed the behaviour of the real and imaginary parts of the calculated polarisation as the gas pressure of nitrous oxide in increased, and as nitrogen is added to provide damping. In Figure 6 we show the calculated behaviour of the real and imaginary parts of the refractive index at low pressure of nitrous oxide with a small pressure of nitrogen added, 6(a, b) and with more nitrogen added as a buffer gas 6(c,d). It may be seen that, when low pressure rapid passage is observed, the real part of the refractive index, 6(a), is distorted as is the imaginary part 6(b). However when collisional damping rate becomes faster that the Rabi cycling both components have their normal behaviour, Figs. 6(c) and 6(d),

Deleted: ())

As the nitrous oxide pressure is increased, the real and imaginary parts show rapid oscillatory structure of the M –structure as line centre is approached. This is shown in figure 7, using the same pressures as for the calculation in Figure 5 (b). At a high pressure of nitrous oxide, 26 mTorr, very large oscillation are shown in the sub-structure associated with the different values of M_J. As the nitrogen is added as a collision partner the rapid oscillatory behaviour is slowly suppressed.

Although the oscillations in the complex refractive index at low pressures of nitrogen are very large, the calculated polarisation shown in Fig 5(b) shows a structure similar to that observed in fig 4(b). This normal behaviour of the calculated polarisation appears to result from cancellation effects due to interference between the oscillatory components of the sub structure shown in Figure 7(a). We believe that the calculated large amplitude oscillatory structure in the complex refractive index shown in Figure 7 is associated with rapid Rabi cycling between the upper and lower states. As the Rabi frequencies will be different owing to the M_J dependence of the effective transition dipole moments, this will lead to interference between the oscillatory components. A theoretical treatment by Horwitz [17] of population transfer made use of the averaging of the Rabi cycling which occurred during the time of the passage through two levels systems.

By comparing the calculated behaviour using the model applied to ethylene, in which the effects of alignment were neglected, with the present model in which it is included, we have verified that the shape of this delayed onset of the switch from absorption to emission is only calculated correctly once M_J alignment has been included in the rapid-passage model.

Deleted:

Deleted: showm

Deleted:

Deleted:

In order to demonstrate that the observation of rapid passage effects is very dependent upon the lack of collisional quenching, we have carried out a series of experiments in which nitrogen is added as a non-absorbing collision partner, with the nitrous oxide playing of role of the chromophore. As nitrogen gas is added to a fixed pressure of nitrous oxide within the absorption cell, the increased collision rate causes dephasing, and quenches the effects of rapid passage. The time between collisions is reduced to 50 ns when 1 Torr of nitrogen is added, and to 0.5 ns when sufficient nitrogen is added to increase the cell pressure to 100 Torr.These effects are shown in Figures 8(a) and 8(b). In 8(a) the pressure of nitrous oxide is very low, and the effects of adding nitrogen are to produce a symmetric pressure broadened line at higher pressure. The decrease in the peak height as the line broadens is similar to that seen in the usual pressure broadening behaviour recorded with low power diode laser or Fourier transform spectrometers. The behaviour of the higher pressure rapid passage spectrum shown in Figure 8 (b) is very different. The first effect of the addition of nitrogen is to increase the peak height, so that as the rapid passage and saturation effects are suppressed, complete absorption is observed at line centre. As further nitrogen is added broadening is then observed.

The calculated behaviour of these absorption lines with an 80 m path length is shown in Figure 9. In 9(a), with a low starting pressure of nitrous oxide pressure, the signals resemble those of figure 8(a). In 9(b) we show calculations of the effects of quenching of the signals when a higher nitrous oxide "chromophore" pressure is used. Initially we used much shorter path lengths of 10 and 20 m for the Maxwell-Bloch calculations. However in order to achieve the same number density we had to increase the nitrous oxide pressure. This produced more collisional damping at

Deleted:

Deleted: lenghts

the higher nitrous oxide pressures so that the pressure dependent time delay of the switch from absorption to emission shown experimentally, Fig. 4 and Fig. 6, was calculated to occur much more rapidly than in the experiments. Only when longer path lengths and lower nitrous oxide pressures were used in the calculations did they match the behaviour seen experimentally. The recovery of the correct form of the pressure broadened line at gas pressure of from 25 to 100 Torr demonstrates that the collision frequency is more rapid that the rate of the frequency downchirp, and "normal" Beer-Lambert absorption occurs.

Deleted: t

The behaviour of the rapid passage signals of the *l*-doublets of nitrous oxide shows clear signals of alignment and of coherent excitation. In Figure 10 the rapid passage signals of the P18 *l*-doublet transition of the $01^{1}1$-$01^{1}0$ band are shown at low and high pressure. In figure 10(a) at low partial pressures of vibrationally excited nitrous oxide, normal rapid passage signals are observed. However at higher partial pressures the signal has a very asymmetric shape, and oscillatory structure is seen in the experimental spectrum.

In Figure 11 we show the calculated response of this type of *l*-doublet, including M_J alignment via the use of a P5 transition but using the *l*-doubling separation of P18, In these calculations we either included, co, or neglected, nc, the coherent interactions between the equivalent M_J components of the two *l*-doublet transitions. At low gas pressures, Figure 11 (a) the response signals with either coherent or incoherent addition were almost identical. However as the pressure of nitrous oxide was increased further, it may be seen in Figure 11 (b) only the calculated spectra in which the effects of coherence were included resembled those of the experiments shown in Figure 10.

Further evidence for the role of number density in determining the type of rapid passage signal seen comes from the observation that rapid passage signals observed in the P or R branches of the ^{15}N and ^{18}O isotopomers resemble those of the P branch lines of the major isotopic form, $^{14}N^{14}N^{16}O$, when the partial pressures are identical. This may be seen in Figure 3(b). Although more nitrous oxide needs to be added in order to detect the weaker lines, the collision frequency is still so low that little collisional damping affects the rapid passage process.

Our final evidence for the occurrence of molecular alignment is the occurrence of free induction decay (FID) signals on the long wavelength side of the emission spike, as the nitrous oxide pressure is further increased up to ca 0.5 Torr, in a cell with a 40 m path length. This is shown in Figure 12. We believe that the switching off of the driving field, allowing the dipoles to precess, may be due to a switch from self-focussing to defocusing, described by Grischowsky [18,19], since the real part of the refractive index associated with this absorption changes sign as the laser sweeps through the absorption line from high to low frequencies.. In Figure 12 it may be seen that the FID modulation frequency increases as the partial pressure of nitrous oxide is slowly increased. The effect of the rapid change in the refractive index on the beam waist, and hence of the power density, is not included directly in the present Maxwell Bloch calculations. However the beam waist of 0.1 mm which we have used in the calculations was chosen to produce the Rabi frequency necessary to induce the effects which we have observed with a laser power of about 30 mW. The effective beam waist, 0.1 mm, is much smaller than the 1/e waist of 1.28 mm calculated for our Herriott cell (see Table 2).

Deleted: figure

Conclusions

We have demonstrated experimentally, and by the use of computer solutions of Maxwell-Bloch equations, in which both Doppler phased array effects and molecular alignment are included, that a frequency swept pulsed quantum cascade infrared laser may produce a large degree of alignment in a low pressure gas such as nitrous oxide. It was also shown that light induced coherent interactions between equivalent M_J transitions of l-doublets could also be demonstrated. The maximum amount of population transfer calculated using a pressure of 0.5 milliTorr is 7.5% for M=1, falling to 1.8 % for M=9. The maximum change in population difference between the levels is then 15%. At these gas pressures there is no calculated loss of the population transferred in 40 ns. When the calculation is repeated with the addition of 1 Torr of nitrogen, the maximum population transfer is 5.5%, and the half life of the decay of the population transferred is 16 ns. When 25 torr of nitrogen is added to the cell the maximum population transferred is 0.25%, as the collision frequency is sufficient to quench the effects of rapid passage.

As spectrometers based on pulsed QC lasers are now widely used for atmospheric measurements [2,5], the results of our analysis may be used to define the operating conditions of the spectrometers such that linear absorption conditions may be maintained.

From the standpoint of molecular dynamics the observation of free induction decay signals shows that the alignment produced in these rapid passage experiments is large enough to be used in the first stage of pump-probe experiments, where a well-aligned sample is required for the first

step of the experiment. This type of sample is often required as the first stage of a vibrational ladder climbing experiment. Future experiments will explore the use of time dependent alignment in pump-probe experiments.

Acknowledgements

The authors would like to thank the United Kingdom Engineering and Physical Research Council (EPSRC) for funding the initial part of this work through the research grant GST/M69111 1999, and for the research studentship for MTM. We are indebted to the Natural Environment Research Council for funding the main part through the research grant NER/T/S/2002/00052 as part of the COSMAS programme, and for the research studentship to S.W.

References:

1. M. T. McCulloch, G. Duxbury and N. Langford, Mol. Phys. 104, 2767-2779 (2006)
2. G. Duxbury, N. Langford, M.T. McCulloch and S. Wright, Chem. Soc. Rev., 34, 1 (2005)
3. R.A. Toth, App. Opt. 32, 7326-7365 (1993)
4. L.S. Rothman, A. Barbe, D.C. Benner, L.R. Brown, C. Camy-Peyret, M.R. Carleer, K. Chance, C. Clerbaux, V. Dana, V.M. Devi, A. Fayt, J.-M. Flaud, R.R. Gamache, A. Goldman, D. Jacquemart, K.W. Jucks, W.J. Lafferty, J.-Y. Mandin, S.T. Massie, V. Nemtchinov, D.A. Newnham, A. Perrin, C.P. Rinsland, J. Schroeder, K.M. Smith, M.A.H. Smith, K. Tang, R.A. Toth, J. Vander Auwera, P. Varanasi, and K. Yoshino. J. Quant Spectrosc. Radiat. Transfer, **82**, 5-, (2003)
5. S. Wright, G. Duxbury and N. Langford, Appl. Phys. B. online 08/2006 doi: 10.1007/s00340-006-2384-x, paper copy 84, (2006)
6. R.R. Ernst, "Advances in Magnetic Resonance (Academic Press, New. York, 1966), vol2, pp 1-135.
7. R.E. Drullinger and R.N. Zare, J.Chem. Phys. 51, 5532-5542 (1969)
8. R.N. Zare, "Angular Momentum: Understanding Spatial Aspects in Chemistry and Physics, Wiley New York (1988)
9. T.Y. Chang in Topics in Applied Physics, ed Y.R. Shen, Vol. 16, 215-272 Springer Verlag Berlin, 1977.
10. M.T. McCulloch, E.L. Normand, N. Langford, G. Duxbury and D.A. Newnham, J. Opt Soc. Am. B, 20, 1761 (2003)
11. J.W. Stoner, D. Szymanski, S.S. Eaton, R.W. Quine, G.A. Rinard and G.R. Eaton, J. Magn. Reson. 170, 127 (2004)
12. L. Allen and J. H. Eberly "Optical Resonance and two level atoms" (Dover, New York, 1975).
13. N. Dam, L. Oudejans and J. Reuss, Chem, Phys. 140, 217-231 (1990)
14. C.H. Townes and A.L. Schawlow, 'Microwave Spectroscopy", (McGraw-Hill, New York, 1955)
15. J. T. McGurk, T.G. Smaltz and W.H. Flygare, J. Chem. Phys. 66, 4181 (1974)
16. J.B. McManus, P.L. Kebabian and M.S. Zahniser, Appl. Opt. 34, 3336 (1995)
17. P. Horwitz, Appl.Phys. Lett. **26**, 306-308 (1974)
18. D. Grischowsky, Phys. Rev. Lett. 24, 866 (1970)
19. D. Grischowsky and J.A. Armstrong, Phys. Rev. A6, 1566 (1972)

Deleted: ,

Table 1
Assignment, intensities and air broadening parameters of observed N_2O Absorption lines

wavenumber /cm^{-1} [a]	Isotopomer	Vibrational Transition	J'	J"	S[b], integrated intensity [b]	γ air (MHz/Torr [c]	γ self (MHz/Torr) [c]
1277.23526	446	3_0^1	8	9	12.70	6.61	8.64
1277.09362	446	$2_1^1\ 3_1^2$ (f)	9	10	2.790×10^{-3}	8.54	8.54
1277.09038	446	$2_1^1\ 3_1^2$ (e)	9	10	2.750×10^{-3}	8.54	8.54
1277.03549	546	3_0^1	9	8	4.314×10^{-2}	6.61	8.84
1276.98006	456	3_0^1	3	4	2.480×10^{-2}	7.11	9.23
1276.93175	456	$2_{2,2}^{2,2}\ 3_0^1$ (f)	22	23	4.314×10^{-2}	5.79	7.42
1276.92702	456	$2_{2,2}^{2,2}\ 3_0^1$ (e)	22	23	4.355×10^{-2}	5.79	7.42
1276.78867	446	$2_1^1\ 3_0^1$ (f)	16	17	9.235×10^{-1}	6.05	7.87
1276.78362	446	$2_1^1\ 3_0^1$ (e)	16	17	9.193×10^{-1}	6.05	7.87
1276.51413	447	3_0^1	15	14	6.330×10^{-3}	6.17	8.05
1276.40232	446	$2_{2,0}^{2,0}\ 3_0^1$ (e)	19	20	5.242×10^{-2}	5.91	7.64
1276.36576	446	3_0^1	9	10	13.55	6.52	8.54
1276.25461	546	3_0^1	8	7	3.992×10^{-2}	6.70	8.75
1276.12731	456	3_0^1	4	5	3.036×10^{-2}	7.00	9.10
1275.92269	456	3_1^2	2	3	1.895×10^{-2}	8.62	9.36
1275.89524	446	$2_1^1\ 3_0^1$ (f)	17	18	9.072×10^{-1}	6.00	7.79
1275.88774	446	$2_1^1\ 3_0^1$ (e)	17	18	9.032×10^{-1}	6.00	7.79
1275.74968	447	3_0^1	14	13	6.250×10^{-3}	6.23	8.14
1275.49287	446	3_0^1	10	11	14.23	6.45	8.43
1275.4705	546	3_0^1	7	6	3.572×10^{-2}	6.79	8.87
1275.27087	456	3_0^1	5	6	3.552×10^{-2}	6.90	8.99
1275.10452	446	$2_{2,2}^{2,2}\ 3_0^1$ (f)	24	25	3.826×10^{-2}	5.73	7.29
1275.10217	446	$2_{2,2}^{2,2}\ 3_0^1$ (e)	24	25	3.859×10^{-2}	5.73	7.29
1275.07831	446	3_1^2	3	4	2.488×10^{-2}	8.60	9.23
1274.99872	446	$2_1^1\ 3_0^1$ (f)	18	19	8.870×10^{-1}	5.95	7.79
1274.98852	446	$2_1^1\ 3_0^1$ (e)	18	19	8.790×10^{-1}	5.95	7.72
1274.76081	448	3_0^1	38	37	8.346×10^{-3}	5.51	6.65
1274.68319	546	3_0^1	6	5	3.137×10^{-2}	6.90	8.99
1274.61651	446	3_0^1	11	12	14.76	6.37	8.33
1274.58026	446	$2_{2,0}^{2,0}\ 3_0^1$ (e)	21	22	4.838×10^{-2}	5.82	7.49
1274.41074	456	3_0^1	6	7	4.024×10^{-2}	6.79	8.87
1274.23062	446	3_1^2	4	5	3.048×10^{-2}	8.59	9.10
Average	pressure	Broadening				6.63	8.26

(a) Refs. [2,3]

(b) Intensities in 10^{-20} cm/molecule

(c) Ref. [3] , values converted from cm^{-1}/Atm. , half width at half height, to MHz/Torr, full width half height.

Table 2
Parameters used the rapid passage calculations

Parameter	Value
Transition dipole moment, μ_{ij}/D	0.1336 [a]
number of time steps	10^5
number of points in the velocity grid	400
Laser power/ milliW.	30
Effective beam waist in cell/mm	0.1
1/e beam waist in cell/mm	1.28
N_2 broadening, full width half maximum, $\gamma_{N_2}/(\text{MHz Torr}^{-1})$	6.4
Self broadening, full width half maximum, $\gamma_{N_2O}/(\text{MHz Torr}^{-1})$	10.02

Representative lines	
Single	P10
l- doublet	P5 effective
doublet splitting/MHz	225

[a] Ref.[3]

Deleted: Beam

Figures

Figure 1

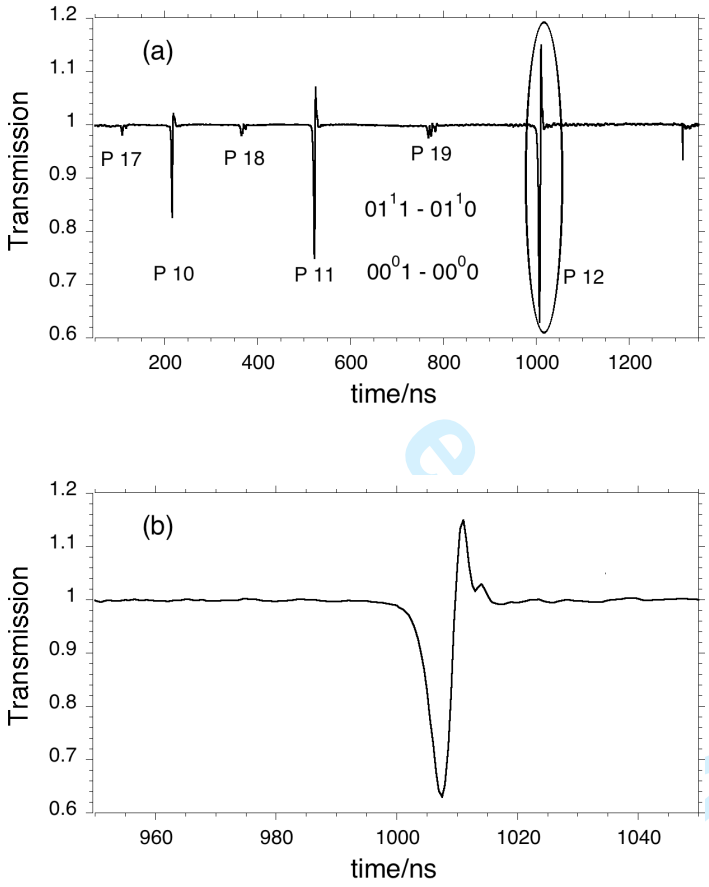

Transmission spectrum of N2O recorded using a path length of 110 m. The gas pressure was 0.6 mTorr, the laser drive current 3.5 A, and the pulse length1270 ns. The time is measured relative to a trigger pulse derived from the control electronics. (a) Full scan, vibration states labelled by $v_1v_2^1v_3$. (b) Expanded plot of the P12 line of the ν_3 band showing the shape of the rapid passage signal.

Figure 2

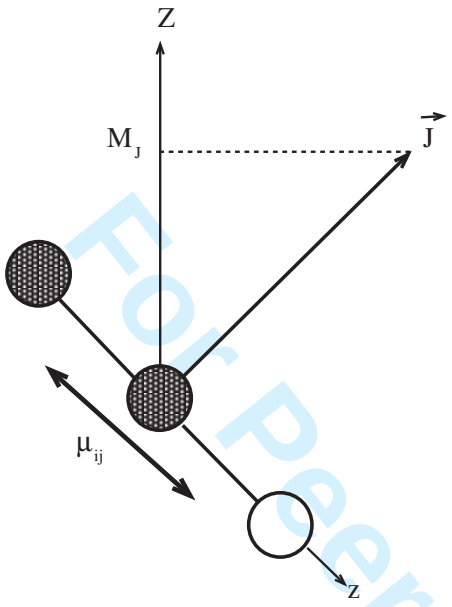

A schematic diagram of the relationship between the direction of the vibrational transition moment along the z-axis, the direction of the angular momentum vextor perpendicular to the z axis, and one of the projections of the total angular momentum, M_J, along the space fixed Z-axis. The laser radiation is linearly polarised, with the electric vector parallel to the Z-axis. The N atoms are represented by filled circles, and the O atom by an open circle.

Figure 3

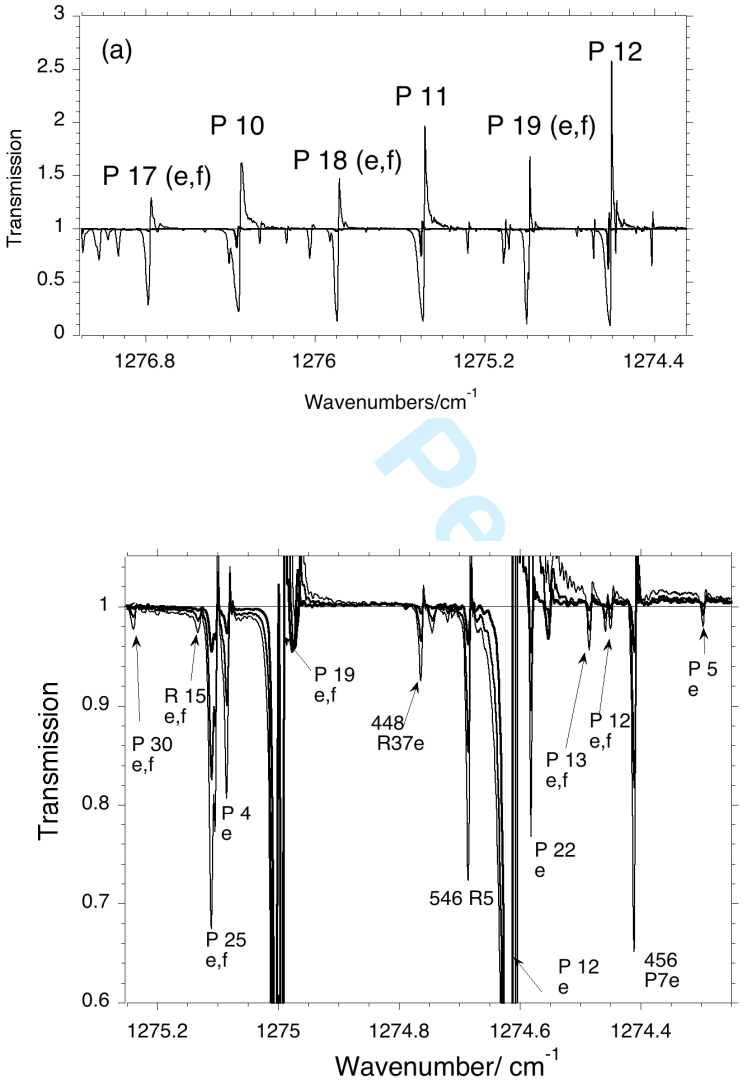

A survey scan showing the assignments of some of the absorption lines within the tuning range of the QC laser. The path length and drive conditions are as in Figure 1. The calibration of the wavenumber scale has been made using the fringes from the germanium

etalon, and the positions of the N_2O lines given by Toth (2). Weak spectrum, a gas pressure of 0.6 mTorr, strongly absorbing spectrum, a gas pressure of 31.3 mTorr. (a) Full scan range, the positions of the main P branch transitions of ν_3, and of the first hot band are indicated. (b) Expanded scale to show the identification of the weaker hot band lines and transitions of the ν_3 transitions of the minor isotopic species. A listing of the assignments of all the identified lines is given in Table 1.

Figure 4

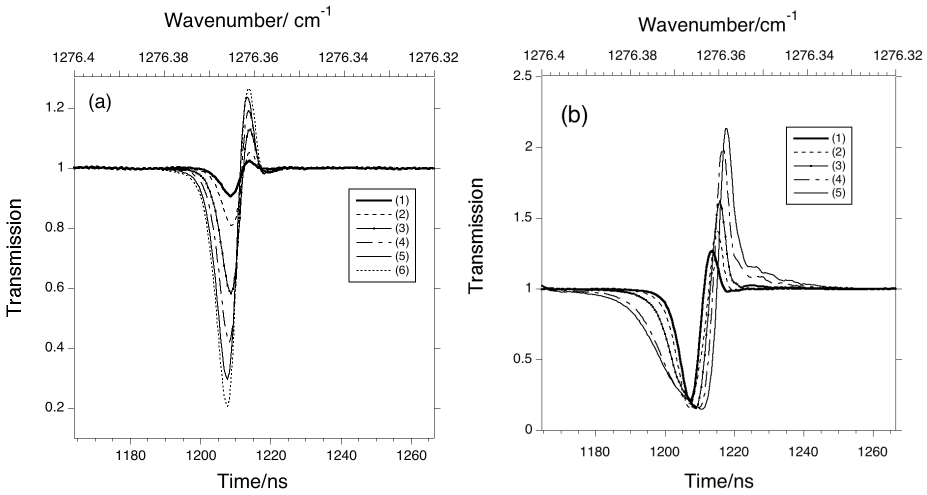

The rapid passage structure of the P10 line of the ν_3 band as a function of increasing pressure of nitrous oxide. The path length used was 110 m, the laser current 2.5 A, and the total sweep range 1.27 microseconds. The average chirp rate of the laser during the passage is 23.4 MHz/ns. The effective resolution is 102 MHz (0.0034 cm^{-1})

(a) low pressure: 1, 0.01 mTorr; 2, 0.1mTorr; 3, 0.2 mTorr; 4, 0.3 mTorr; 5, 0.4 mTorr and 6, 0.5 mTorr.

(b) High pressure: 1, 0.5 mTorr; 2, 1 mTorr; 3, 2.2 mTorr; 4, 6.2 mTorr and 5, 9.3 mTorr.

Deleted:

Deleted:

Figure 5

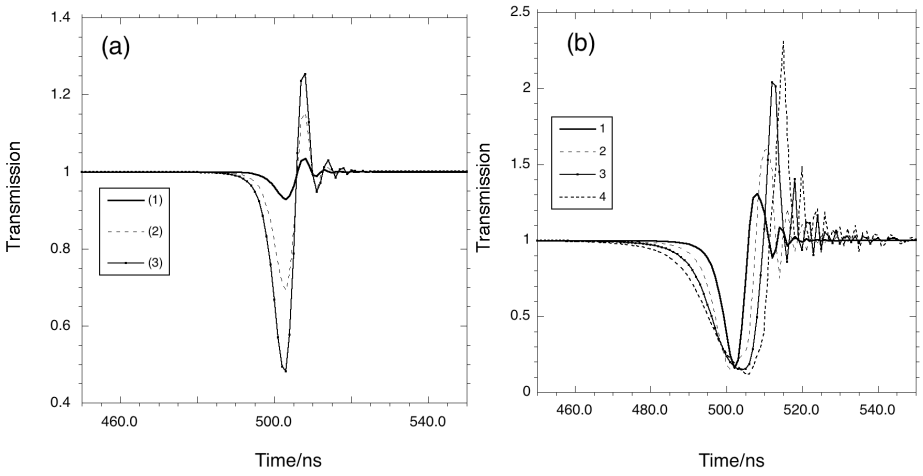

The calculated rapid passage structure of the P10 line of the ν_3 band of nitrous oxide as a function of increasing pressure of nitrous oxide. The details of the parameters used in the Maxwell-Bloch calculations are given in Table 2, the path length used was 80 m. (a) low pressure region: (1) 0.05 mTorr; (2), 0.25 mTorr; (3) 0.5 mTorr. (b) high pressure region: (1)1.25 mTorr; (2), 5 mTorr; (3) 12.5 mTorr; (4) 25 mTorr.

Deleted: 1
Deleted: 5
Deleted: 10
Deleted: 25
Deleted: 100
Deleted: 250
Deleted: 500

Figure 6

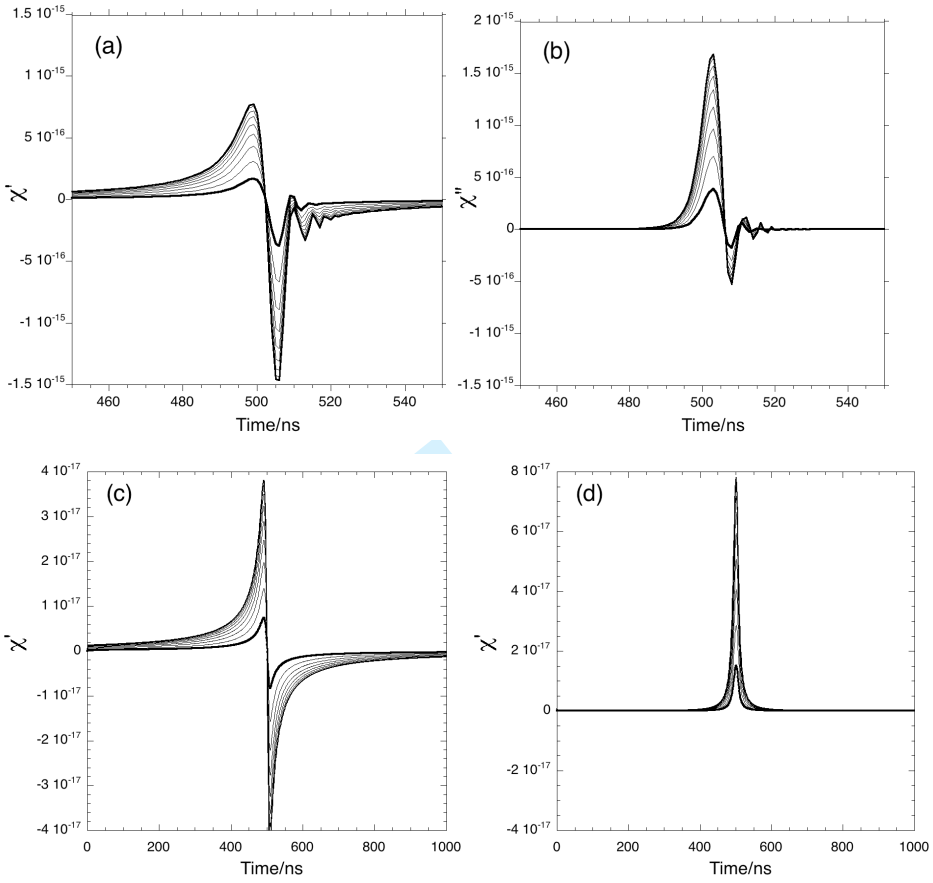

The effects of nitrogen collisions on the shape of the real, χ', and imaginary, χ'', components of the complex refractive index, using the parameters given in Table 2.

(a) χ' and (b) χ'' for a nitrous oxide pressure of 0.05 mTorr and a nitrogen pressure of 5 Torr.

(c) χ' and (d) χ'' for a nitrous oxide pressure of 1 mTorr and a nitrogen pressure of 25 Torr.

Deleted: 1

Figure 7

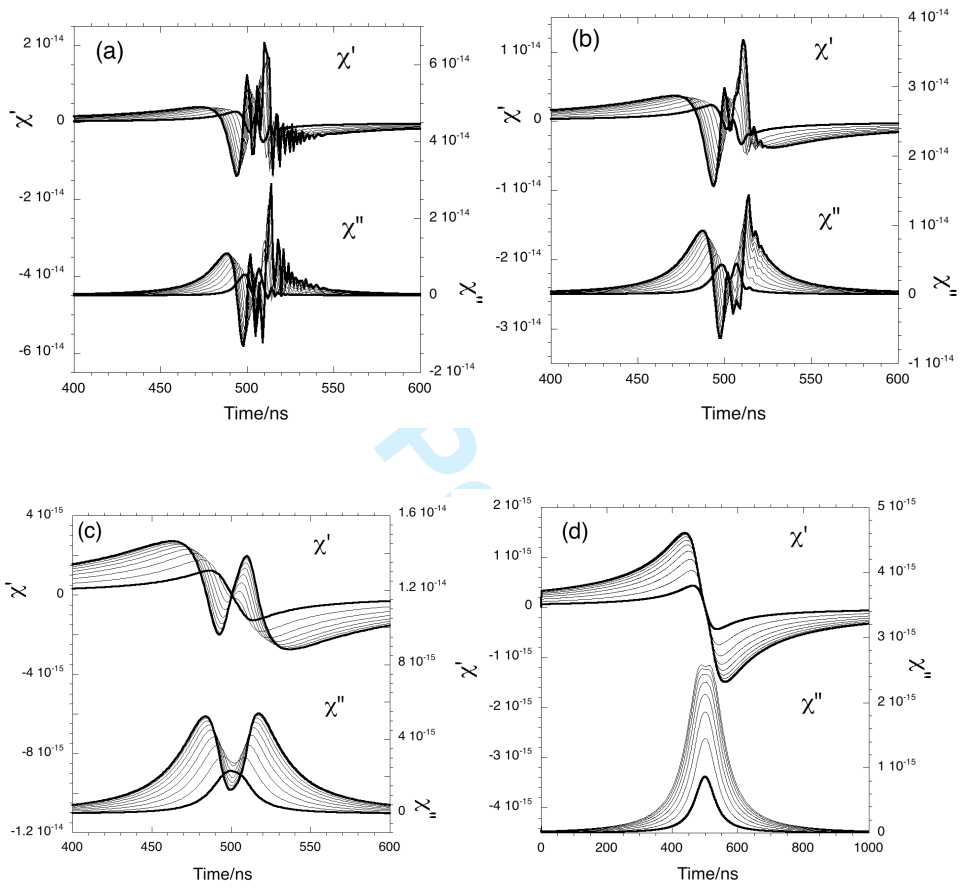

The effects of nitrogen collisions on the shape of the real, χ', and imaginary, χ'', components of the complex refractive index when a high pressure of N_2O, 1.25 mTorr is used. These are the conditions used for Fig. 5(b).The parameters used for the calculation are given in Table 2.

(a) N_2 1 Torr, (b) N_2 5 Torr , (c) N_2 25 Torr and (d) N_2 100 Torr .

Note that with this degree of non-linear driving the normal form of the real and imaginary parts of the complex refractive index is not achieved until 100 Torr of nitrogen is added to provide very large collisional damping.

Deleted: 25

Figure 8

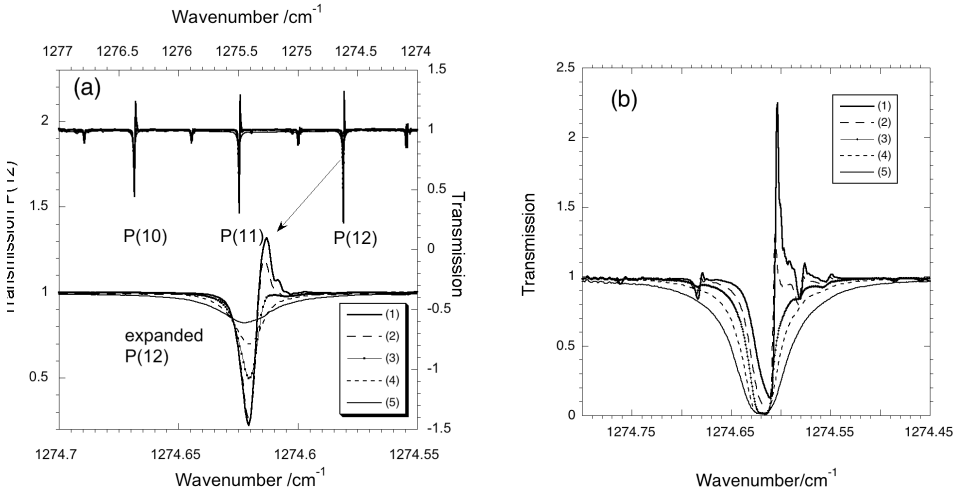

The effect of adding nitrogen, as a collision partner, on the shape of the rapid passage signals. The path length used was 110 m, the laser current 3.5 A, and the total sweep range 1.27 microseconds.

(a)

Top entire spectrum, bottom an expanded scale to show the change in the shape of the rapid passage signal with addition of nitrogen as a buffer gas. In the region of P12 absorption line the average chirp rate of the laser during the passage is 40 MHz/ns. The effective resolution is 132 MHz (0.0044 cm^{-1})

1, initial N_2O pressure 0.6 mTorr; 2 , N_2 added to a total pressure of 4.5 Torr; 3 N_2 added to a total pressure of 20 Torr; 4, N_2 added to a total pressure of 50 Torr; 5, N_2 added to a total pressure of 102 Torr

(b) The effect of collisions with nitrogen on the shape of the P12 rapid passage signal when a much larger N_2O "chromophore" pressure is used, the laser parameters are as Figure 6a. 1, initial N_2O pressure 13.3 mTorr; 2 , N_2 added to a total pressure of 5 Torr; 3 N_2 added to a total pressure of 27 Torr; 4, N_2 added to a total pressure of 56 Torr; 5, N_2 added to a total pressure of 102 Torr

Figure 9

Deleted:

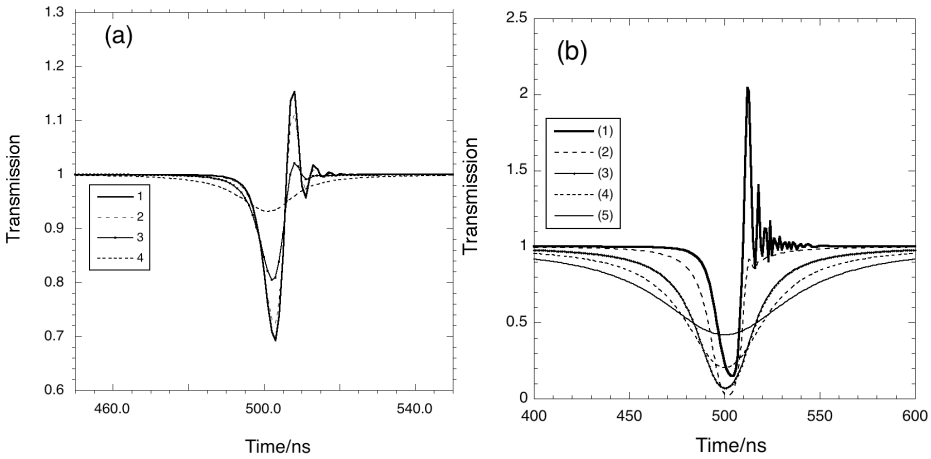

The effects of nitrogen collisions on calculated rapid passage structure of the P10 line of the ν_3 band of nitrous oxide at a fixed pressure of nitrous oxide. The details of the parameters used in the Maxwell-Bloch calculations are given in Table 2, the path length used was 80 m. (a) low pressure: 1, initial N_2O pressure 0.25 mTorr; 2 , 1 Torr of N_2 added; 3 , 5 Torr of N_2 added; , 25 Torr of N_2 added (b) high pressure,(1), initial N_2O pressure 12.5 mTorr, high pressure: (1), (2) , 5 Torr of N_2 added; (3) , 25 Torr of N_2 added; (4) , 50 Torr of N_2 added; (5), 100 Torr of N_2 added.

Deleted: 5

Deleted: ¶

Figure 10

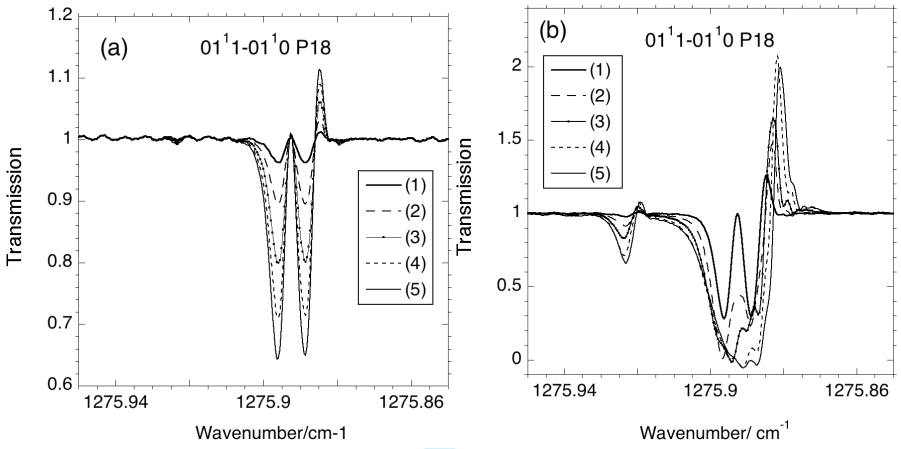

The effects of alignment and coherence on the structure of the rapid passage structure of the 01^11- 01^10 P18 *l*-doublet, whose transitions are separated by 225 MHz. . In the region of this doublet the average chirp rate of the laser during the passage is 23.2 MHz/ns. The effective resolution is 101 MHz (0.0034 cm^{-1})

(a) low pressure region: 1, 1.9 mTorr; 2, 3.9mTorr; 3, 5.8 mTorr; 4, 7.7 mTorr; 5, 9.6 mTorr,

(b) high pressure region: 1, 60 mTorr; 2, 160mTorr; 3, 210 mTorr; 4, 310 mTorr; 5, 400 mTorr,

Figure 11

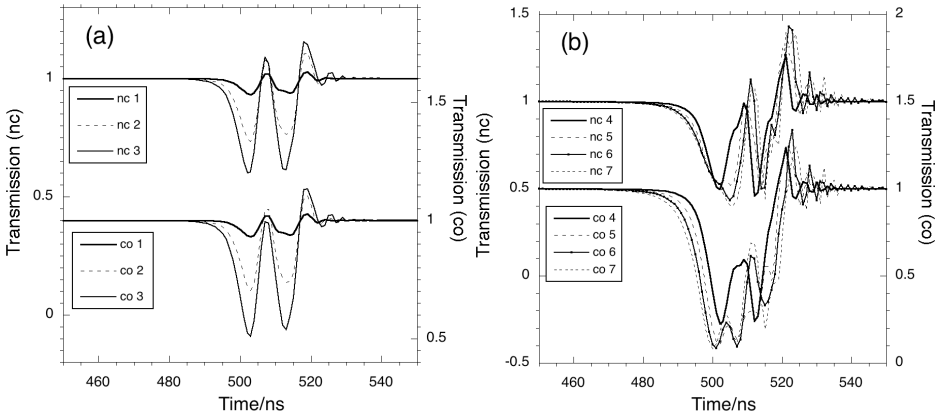

The calculated effects of alignment and coherence on the structure of the rapid passage structure of an *l*-doublet of a P branch line the $01^{1}1$- $01^{1}0$ band, assuming that the transitions are separated by 225 MHz. The main calculation details are given in Table 2. The value of J" was set at 5 to minimise the time taken by the calculation. co indicates that the contributions of equivalent M_J components of the *l*-doublet are added coherently, nc indicates no coherence effects are included.

(a) low pressure region: 1, 1 mTorr; 2, 5 mTorr; 3, 10 mTorr;

(b) high pressure region: 1, 25 mTorr; 2, 50mTorr; 3, 75 mTorr; 4, 100 mTorr

Pressures used in this calculation are the partial pressures related to the number density of the molecules in the vibrationally excited lower state, and hence are much lower than the total gas pressures given in Figure 9.

Figure 12

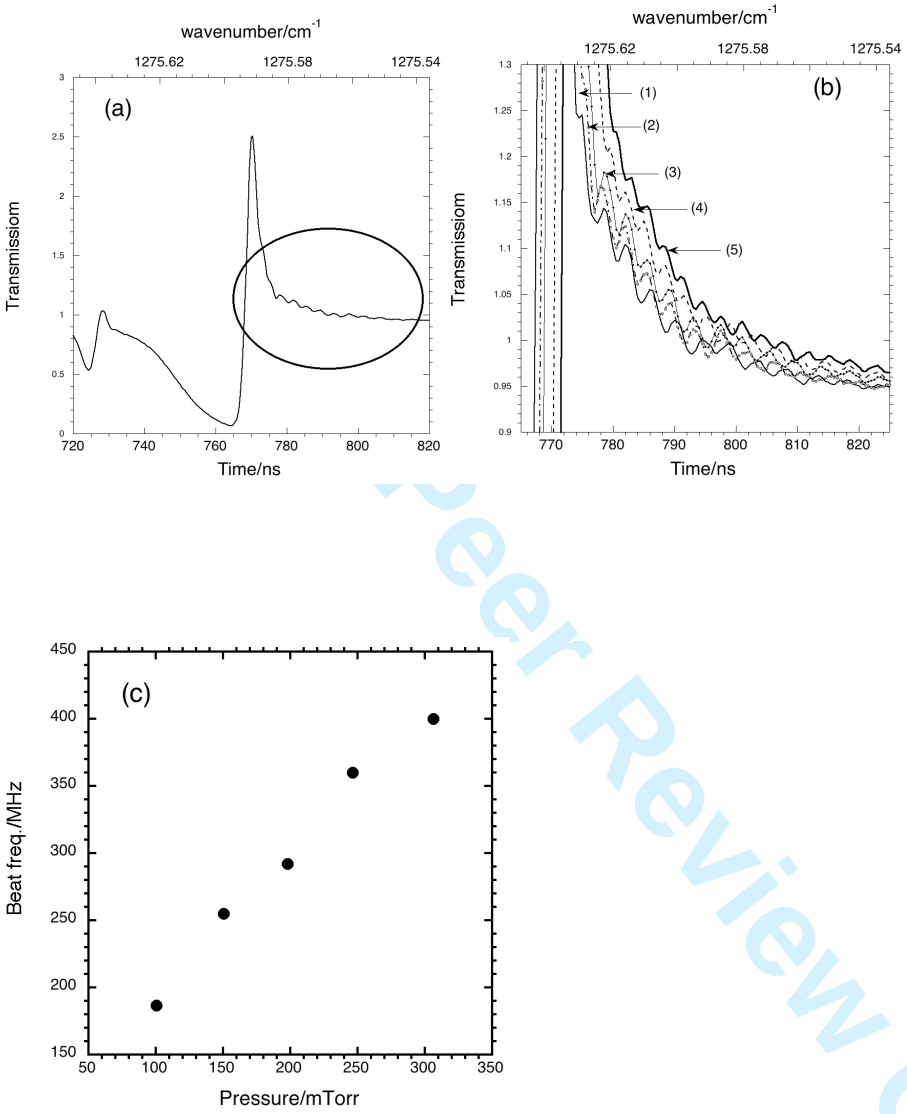

The observation of free induction decay, (FID), signals when very high pressures of nitrous oxide are interrogated within the long pathlength cell. The pathlength used was 40 m, the laser current 3.5 A, and the total sweep range was 1.27 microseconds.

(a) An overview of the region covering the rapid passage signal of the P11 line of nitrous oxide. The gas pressure used was 181 mTorr. The region in which the FID structure is seen is indicated on the low frequency side of the large emission signal.

(b) An expanded plot of the region indicated on Fig11 (a) where several FID signals are shown. The gas pressures are (1), 161 mTorr; (2), 181 mTorr;, (3) 199 mTorr, (4), 247 mTorr and (5), 310 mTorr.

(c) A plot showing the almost linear variation of the beat frequency associated with the FID signal as the pressure of nitrous oxide is increased.

Deleted: